# Oxygen Pressure-Tuned Epitaxy and Magnetic Properties of Magnetite Thin Films

Junran Zhang,[1] Wenqing Liu,[2] Minhao Zhang,[1] Xaoqian zhang,[1] Wei Niu,[1] Ming Gao,[1] Xuefeng Wang,[1,a)] Jun Du,[3] Rong Zhang,[1] and Yongbing Xu[1,2,a)]

[1] *Jiangsu Provincial Key Laboratory of Advanced Photonic and Electronic Materials, Collaborative Innovation Center of Advanced Microstructures, School of Electronic Science and Engineering, Nanjing University, Nanjing 210093, China*

[2] *York-Nanjing Joint Centre (YNJC) for spintronics and nano engineering, Department of Electronics, The University of York, YO10 3DD, United Kingdom*

[3] *School of Physics, Nanjing University, Nanjing 210093, China*

## Abstract

Quasi-two-dimensional $Fe_3O_4$ epitaxial thin films have been synthesized by pulsed laser deposition technique at six fixed oxygen pressures of 0, $1\times10^{-5}$, $5\times10^{-5}$, $1\times10^{-4}$, $5\times10^{-4}$, and $1\times10^{-3}$ mbar. The film obtained under high vacuum ($\sim1\times10^{-8}$ mbar) hosts a large magnetoresistance of about 11.5 % at 9 T and 100 K. In addition, oxygen-pressure-dependent saturation magnetizations of the films are as large as that of the bulk $Fe_3O_4$. A trivial change in oxygen stoichiometry of $Fe_3O_4$ is found crucial for the ferrimagnetic order at room temperature. Possible mechanisms of ferrimagnetic order driven by change in oxygen stoichiometry are discussed.

## *Keywords*:

Fe3O4 film, oxygen stoichiometry, magnetoresistance, magnetization, ferrimagnetic order

In the contemporary spintronics research, magnetite, especially in nano-form, has attracted enormous interest due to its great potential for information technology. To synthesize highly spin polarized materials as spin sources and to combine them with semiconductors, which can be easily integrated with current magnetic technologies are prerequisites for proposed spintronics devices such as the spin field effect transistor (SFET).[1] As a model half-metallic material, $Fe_3O_4$ has shown 80% spin polarization near the Fermi level in experiment[2] and theoretically, up to 100% can be expected.[3] More desirably, the high Curie temperature of $Fe_3O_4$ makes it a promising candidate for room temperature use. Fascinating properties of spin transport have also been presented in $Fe_3O_4$, i.e., spin Seebeck effect,[4] spin filter effect,[5] gate voltage-induced phase transition,[6] and spin valve effect of $Fe_3O_4/MgO/Fe_3O_4$ junctions.[7] Yet at the meantime, many fundamental properties of magnetite, such as the half-metallicity, spin and orbital ordering, Verwey transition mechanism and the coupling mechanism between different sites have long been open issues, and with the $Fe_3O_4$ synthesized under different oxygen pressure, these issues become even more sophisticated.

Magnetite is believed to have a cubic inverse spinel structure, where $Fe^{3+}$ ions occupy tetrahedral sites (usually called A sites), whereas octahedral sites (B sites) are occupied by both $Fe^{3+}$ and $Fe^{2+}$ ions. The spin of $Fe^{3+}$ ions at octahedral and tetrahedral sites are aligned antiparallel to each other leading to a net magnetic moment of 480 emu/g (4 $\mu$B/f.u.), corresponding to a fully occupied local majority band (opposite for A and B sites). The presence of integer magnetic moment of magnetite is expected in experiment as indication for a B-site minority electron conduction mechanism, and its accompanied full spin polarization at the Fermi level. However, controversial results of it have been reported varies from 300 emu/g by Nagahama et al. using molecular beam epitaxy (MBE) under oxygen pressure[8] to 1094 emu/g by Orna et al. using pulsed laser deposition (PLD) under pure vaccum.[9] Table I summaries some of the experimental efforts toward this issue.

Over the one-century's research on magnetite, there exists wide-spread recognition that further insights into open problems relating to magnetite are obtainable only by means of bulk, single crystals of perfect stoichiometry, grown in accordance with optimum preparation rules and phase diagrams. This, in one respect, strongly depends on the accurate controlling of the oxygen pressure, not only during maintenance of the thermodynamic high-temperature equilibrium, but also-most importantly-during cooling down to room-temperature. Violation of this precept-by uncontrolled quenching of the sample, as is often practiced at the end of tempering-causes considerable loss of crystal quality, as shown in several reports.[9-14] The magnetization of $Fe_3O_4$ thin films grown by PLD can be tuning by oxygen partial from $0.4\times10^{-6}$ to $10\times10^{-6}$ Torr.[10] Seki et al. grew Ge-substituted $Fe_3O_4$ thin films under high oxygen pressures (0.01-0.6 Pa) and yielded a spin polarization of 0.50 at room temperatur.[11] However, $Fe_3O_4$ epitaxial thin films with giant magnetic moment, which comes from the spin of Fe ions

in the tetrahedron site switching parallel to the Fe ions in the octahedron site at the surface, interface, and grain boundaries, were grown in pure vacuum by PLD.[9,15] The influence of oxygen pressure on the quality of $Fe_3O_4$ thin film by PLD is unclear.

In this work, we present systematic investigation of oxygen-pressure-dependent magnetoresistance (MR) and magnetic moment, aiming to contribute to the open question of the magnetic moments of the $Fe_3O_4$ thin film. Quasi-two-dimensional (quasi-2D) $Fe_3O_4$ thin films (~100 nm) were deposited on MgO (001) substrates by PLD. First, a sharp MgO (001) surface was obtained after annealed in vacuum atmosphere for 8 hours at 600 ºC as identified from the reflection high-energy electron diffraction (RHEED) pattern shown in Fig. 1(a). The films were grown at about 410 ºC and six different fixed oxygen pressures atmosphere (0, $1\times10^{-5}$, $5\times10^{-5}$, $1\times10^{-4}$, $5\times10^{-4}$, and $1\times10^{-3}$ mbar). Prior to film deposition, the chamber was pumped down to ~$1\times10^{-8}$ mbar. *In situ* and *real time* monitoring of the growth was performed by RHEED. All films were characterized by X-ray photoelectron spectroscopy (XPS, PHI 5000 VersaProbe), and laser Raman spectrometer (JY HR800). MR and resistance-temperature (R-T) curves were measured by Physical Property Measurement System (PPMS, Quantum Design, Inc.). The magnetic properties of the samples were measured at room temperature using a vibrating sample magnetometer (VSM).

The dot-array and long-line-array in RHEED patterns stand for three dimension (3D) and quasi-2D surface structure and morphology, respectively.[16] $Fe_3O_4$/MgO with quasi-2D surface structure and morphology was shown in Fig. 1(b), which reveals that the surface quality of our $Fe_3O_4$ thin films prepared by PLD is as high as films grown by MBE.[17,18] Due to the fact that the lattice constant of $Fe_3O_4$ (*a*=8.3987 Å) is twice of MgO (*a*=4.212 Å),[19] the emerging patterns of line 2 and 4 in the middle of line 1,3 and 5 are pattern of $Fe_3O_4$. In order to study the surface structure of $Fe_3O_4$ thin film depending on oxygen partial pressure, *in situ* and *real time* RHEED was monitoring during growth of the 6 samples. As we can see from Fig. 1(c), the distances ratio between line 2 and 3 from Fig. 1(b) are invariable and the line width of line 2 increased as oxygen pressure increasing. This means that the phase of $Fe_3O_4$ become weak as oxygen pressure increasing. These phenomena can be explained by some $Fe_2O_3$ phases generated as oxygen pressure increasing. In order to confirm the $Fe_2O_3$ phase, the XPS and Raman were investigated.

Fig. 2(a) is the XPS spectra of $Fe_3O_4$ thin films grown at six different oxygen pressures, inset is the enlargement of the area in dashed line box. The typical Fe $2p_{3/2}$ and Fe $2p_{1/2}$ are observed at ~710 and ~723 eV, respectively. It is known that FeO has a clear satellite feature at ~715.5 eV, and $Fe_2O_3$ has a satellite feature at ~719.1 eV. Such satellite structures are frequently used as fingerprints to identify the other iron oxide phases.[17] One can clearly see that with the exception of the sample grown at pure vacuum, the XPS spectra for all the other $Fe_3O_4$ thin films show signs for satellite structures of $Fe_2O_3$ phase and all films show no signs

for satellite structures of FeO phase. The intensity of the satellite structures of $Fe_2O_3$ phase become stronger as the oxygen pressure increasing. This phenomenon is not completely accord with the report by Liu et al.,[17] in which $Fe_3O_4$ thin films grown by MBE at 8 different oxygen partial pressure (from $1\times10^{-5}$ to $5\times10^{-8}$ mbar), and with the exception of sample grown at the low $5\times10^{-8}$ mbar oxygen partial pressure shown the sign for FeO, all the other samples show no signs for $Fe_2O_3$ and FeO.

Raman is also investigated to confirm the $Fe_2O_3$ phase as shown in Fig. 2(b). Considering the space group $O_h^7$(Fd3m), theory predicts the following modes by proper irreducible representation:[20]

$$A_{1g} + E_g + T_{1g} + 3T_{2g} + 2A_{2u} + 2E_u + 5T_{1u} + 2T_{2u}.$$

The $T_{1g}$, $A_{2u}$, $E_u$, and $T_{2u}$ are silent. Thus there are five Raman active modes ($A_{1g}+E_g+3T_{2g}$) and five infrared active modes ($5T_{1u}$). At room temperature, we observe three modes: the strongest $A_{1g}$ mode at ~675 cm$^{-1}$ and $T_{2g}$(2) and $T_{2g}$(3) modes at ~550 and ~320 cm$^{-1}$, respectively. This is corresponding with the reference.[21] However, with exception of sample grown at the pure vacuum, all other samples show the $A_{1g}$ peaks of $Fe_2O_3$ at ~210 and 480 cm$^{-1}$.[22] XPS and Raman spectroscopies confirm formation of single magnetite phase for the low oxygen pressures and a mixed phase composed of $Fe_3O_4$ and $Fe_2O_3$ for the high pressure.

The magnetic transport properties of films were investigated, which schematic structure for magnetotransport measurements in $Fe_3O_4$ films is shown in Fig.3(a). The R-T of the films were measured as shown in Fig. 3(b). It can be see that a suddenly increase of the resistivity was observed at ~110 and ~124 K for $Fe_3O_4$ films grown at pure vacuum and oxygen partial pressure of $1\times10^{-5}$ mbar, respectively, corresponding to the Verwey transition.[23] Inset of Fig 3(b) is log resistance versus the inverse temperature of $Fe_3O_4$ films grown at pure vacuum, which can see the Verwey transition obviously. At the same temperature, the resistance of $Fe_3O_4$ film grown at pure vacuum is smaller than $Fe_3O_4$ film grown at oxygen pressure of $1\times10^{-5}$ mbar, which possibly attributed to the $Fe_2O_3$ phase generated due to oxygen partial pressure. Fig.3(c) and (d) show the MR measurements at different temperatures for the $Fe_3O_4$ thin films grow at pure vacuum and oxygen pressure of $1\times10^{-5}$ mbar with the magnetic field applied perpendicular to the film plane. As we can see, a large MR value of 11.5 % at 100 K and 9 T is observed, which is larger than references reported.[24,25]

In spite of $Fe_3O_4$ thin films grown in oxygen pressures exist $Fe_2O_3$ phase, magnetic hysteresis loops are observed for all the samples as shown in Fig. 4. The hysteresis loops are obtained at room temperature for five of the samples. As we can see from Fig. 4(a), the large saturation magnetization ($M_S$) of 425 emu/cm$^3$ approaching at the principle bulk-like magnetite saturation value[26] (480 emu/cm$^3$ or 4.0 $\mu_B$/f.u.) is observed by the sample grown at

pure vacuum, which is larger than $Fe_3O_4$ thin films reported by Arora et al.[27] and Orna et al.[9] with same thickness. The saturated magnetic moment decreased due to $Fe_2O_3$ impurities phase generated as increasing the pressure of oxygen as shown in Fig. 4(d), which is extracted from Fig. 4(a) and (b). Both coercivities of in plane and out plane are invariable as oxygen pressure increasing. Fig. 4(c) shows the loops measured in plane and out plane of sample grown at pure vacuum. It is can be seen that the sample exhibits an unobvious out of plane anisotropy, which reveal the high quality of our films.

Arora et al.[27] reveal that the noncompensation of spin moments between the tetrahedral and octahedral sublattices at the surface are inferred to be the main factor contributing to the observed enhanced magnetic moment. Orna et al.[9] reveal that the origin of the enhanced magnetic moment is not intrinsic to magnetite but due to the presence of Fe impurities in the MgO substrates. Oxygen vacancies on electronic structure also can enhance magnetic moment as reported by Jaffari et al..[28] For $Fe_3O_4$ double exchange interaction between $Fe^{3+}$ and $Fe^{2+}$ in octahedral site leads key role which produces ferromagnetic component.[29] In addition, antiferromagnetic super-exchange interaction between octahedral $Fe^{3+}$ and tetrahedral $Fe^{3+}$ cancels each other, retaining net moment of $Fe^{2+}$ to be 4 $\mu$B/f.u.. Recent density of states calculations suggests reduction of moment locally due to oxygen vacancies, although total moment of the crystal remains unchanged.[30] In the current studies surface effect is rather less effective because of significantly large film thickness (~100 nm).[31] Strain is one of the key parameters which can influence magnetization significantly for films including magnetite.[32,33] A significant compressive strain is developed at the sample substrate interface because of lattice mismatch between MgO and $Fe_3O_4$. The strain increases further with oxygen deficiency and it might be involved with the larger number of oxygen defects at the interface for low oxygen partial pressure. A small change in oxygen stoichiometry is suggested to be correlated to the modification and drives a significant change in ferrimagnetic order.

In summary, we have successfully grown the quasi-2D $Fe_3O_4$ epitaxial thin films at different oxygen pressures by PLD. XPS and Raman spectroscopies confirm formation of single $Fe_3O_4$ phase for the low oxygen pressures and a missed phase composed of $Fe_3O_4$ and $Fe_2O_3$ phase for the high oxygen pressures. Oxygen stoichiometry of $Fe_3O_4$ film is found vital for ferromagnetic order.

**Acknowledgements**

| Method | Substrate | Thickness | MR (%) | Oxygen Pressure (mbar) | $M_s$ | Reference |
|---|---|---|---|---|---|---|
| PLD | MgO(100) | 100 nm | 11.5 % | Pure vaccum | 425 emu/cm$^3$ | Our work |
| PLD | GaAs(100) | - | 22 % | Pure vaccum | 430 emu/cm$^3$ | [34] |
| PLD | ZnO/Al$_2$O$_3$(0001) | 70 nm | - | Pure vaccum | 380 emu/cm$^3$ | [35] |
| PLD | SrTiO$_3$(001) | - | - | Pure vaccum | 400 emu/cm$^3$ | [13] |
| PLD | YSZ(111) | - | - | $2\times10^{-6}$ | 400-460 emu/cm$^3$ <br> 480 (Anneal) emu/cm$^3$ | [36] |
| PLD | SrTiO3(100) | >15 nm <br> 3nm | - | Pure vaccum | Close to 480 emu/cm$^3$ <br> 1017 emu/cm$^3$ | [15] |
| PLD | MgO(001) | >20nm <br> 2.8nm | - | Pure vaccum | 349±41 emu/cm$^3$ <br> About 1094 emu/cm$^3$ | [9] |
| PLD | MgO(100) | 10 nm | 3% | Adequate oxygen pressure | - | [37] |
| PLD | MgO(111) <br> MgO(100) | 40 nm | 5% <br> 12 % | $7.8\times10^{-6}$ | 470 emu/cm$^3$ <br> 400 emu/cm$^3$ | [25] |
| PLD | MgO/GaAs(100) | - | - | $5\times10^{-5}$ | 400 emu/cm$^3$ | [26] |
| PLD | Si(100) | - | - | $0.4\times10^{-6}$ <br> $4\times10^{-6}$ | 0.45 $\mu$B/f.u. <br> 0.2 $\mu$B/f.u. | [10] |
| MBE | MgO(100) | - | - | $1\times10^{-6}$ | 300 emu/cm$^3$ | [8] |
| MBE | MgO(001) | 10 nm | 0.3% | $6.6\times10^{-6}$ | - | [38] |
| MBE | MgO(001) | 1.5 $\mu$m | - | Oxygen plasma | 300 emu/cm$^3$ | [39] |
| MBE | MgO(001) | 60 nm | 5% | Oxygen plasma | - | [40] |
| MBE | MgO(001) | 5nm <br> 20 nm | - | Oxygen plasma | 922 emu/cm$^3$ <br> 613 emu/cm$^3$ | [41] |
| MBE | GaN(0001) | 6 nm <br> 3nm | - | $8\times10^{-4}$ | 450 emu/cm$^3$ <br> 350 emu/cm$^3$ | [42] |

**TABLE 1.** MR and $M_s$ of Fe$_3$O$_4$ films grown at different conditions of our sample and those from the literatures.

# References

[1]   S. Datta and B. Das, Appl. Phys. Lett. **56**, 665 (1990).

[2]   Y. S. Dedkov, U. Rüdiger, and G. Güntherodt, Phys. Rev. B **65**, 064417 (2002).

[3]   V. Antonov, B. Harmon, and A. Yaresko, Phys. Rev. B **67**, 024417 (2003).

[4]   R. Ramos, T. Kikkawa, K. Uchida, H. Adachi, I. Lucas, M. Aguirre, P. Algarabel, L. Morellón, S. Maekawa, and E. Saitoh, Appl. Phys. Lett. **102**, 072413 (2013).

[5]   Z. M. Liao, Y. D. Li, J. Xu, J. M. Zhang, K. Xia, and D. P. Yu, Nano Lett. **6**, 1087 (2006).

[6]   J. Gooth, R. Zierold, J. G. Gluschke, T. Boehnert, S. Edinger, S. Barth, and K. Nielsch, Appl. Phys. Lett. **102**, 073112 (2013).

[7]   H. C. Wu, O. N. Mryasov, M. Abid, K. Radican, and I. V. Shvets, Sci. Rep. **3**, 1830 (2013).

[8]   T. Nagahama, Y. Matsuda, K. Tate, T. Kawai, N. Takahashi, S. Hiratani, Y. Watanabe, T. Yanase, and T. Shimada, Appl. Phys. Lett. **105**, 102410 (2014).

[9]   J. Orna, P. A. Algarabel, L. Morellón, J. A. Pardo, J. M. de Teresa, R. López Antón, F. Bartolomé, L. M. García, J. Bartolomé, J. C. Cezar, and A. Wildes,   Phys. Rev. B **81,** 144420 (2010).

[10]  K. Dey, A. Ghosh, P. Modak, A. Indra, S. Majumdar, and S. Giri, Appl. Phys. Lett. **105**, 142905 (2014).

[11]  M. Seki, M. Takahashi, T. Ohshima, H. Yamahara, and H. Tabata, Appl. Phys. Lett. **103**, 212404 (2013).

[12]  M. Ishikawa, H. Tanaka, and T. Kawai, Appl. Phys. Lett. **86**, 2504 (2005).

[13]  Q.X. Zhu, M. Zheng, M.M. Yang, R.K. Zheng, Y. Wang, X.M. Li, and X. Shi, Appl. Phys. Lett. **105**, 241604 (2014).

[14]  J. Dho, Appl. Phys. Lett. **106**, 202405 (2015).

[15]  X. Guan, G. Zhou, W. Xue, Z. Quan, and X. Xu, APL Materials **4**, 036104 (2016).

[16]  A. Ichimiya and P. I. Cohen, *Reflection high-energy electron diffraction*. (Cambridge University Press, 2004).

[17]  X. H. Liu, A. D. Rata, C. F. Chang, A. C. Komarek, and L. H. Tjeng, Phys. Rev. B **90,** 125142 (2014).

[18] Z. Ding, B. L. Chen, J. H. Liang, J. Zhu, J. X. Li, and Y. Z. Wu, Phys. Rev. B **90,** 134424 (2014).

[19] D. Margulies, F. Parker, M. Rudee, F. Spada, J. Chapman, P. Aitchison, and A. Berkowitz, Phys. Rev. Lett. **79**, 5162 (1997).

[20] J. Verble, Phys. Rev. B **9**, 5236 (1974).

[21] D. M. Phase, S. Tiwari, R. Prakash, A. Dubey, V. G. Sathe, and R. J. Choudhary, J. Appl. Phys. **100**, 123703 (2006).

[22] C. Baratto, P. Lottici, D. Bersani, G. Antonioli, G. Gnappi, and A. Montenero, J. Sol-Gel Sci. Techn. **13**, 667 (1998).

[23] E. J. W. Verwey, Nature **114**, 327 (1939).

[24] A. Ramos, J.B. Moussy, M.J. Guittet, A. Bataille, M. Gautier-Soyer, M. Viret, C. Gatel, P. Bayle-Guillemaud, and E. Snoeck, J. Appl. Phys. **100**, 103902 (2006).

[25] O. Chichvarina, T. S. Herng, W. Xiao, X. Hong, and J. Ding, J. Appl Phys **117**, 17D722 (2015).

[26] W. Q. Liu, Y. B. Xu. P. K. J. Wong, N. J. Maltby, S. P. Li, X. F. Wang, J. Du, B. You, J. Wu, P. Bencok, and R. Zhang Appl. Phys. Lett. **104**, 142407 (2014).

[27] S. K. Arora, H.C. Wu, R. Choudhary, I. Shvets, O. Mryasov, H. Yao, and W. Ching, Phys. Rev. B **77**, 134443 (2008).

[28] G. H. Jaffari, A. K. Rumaiz, J. C. Woicik, and S. I. Shah, J. Appl. Phys. **111**, 093906 (2012).

[29] J. B. Moussy, J. Phys. D: Appl. Phys. **46**, 143001 (2013).

[30] R. Arras, L. Calmels, and B. Warot-Fonrose, Appl. Phys. Lett. **100**, 032403 (2012).

[31] M. Fonin, R. Pentcheva, Y. S. Dedkov, M. Sperlich, D. V. Vyalikh, M. Scheffler, U. Rüdiger, and G. Güntherodt, Phys. Rev. B **72**, 104436 (2005).

[32] S. Jain, A. Adeyeye, and D. Dai, J. Appl. Phys. **95**, 7237 (2004).

[33] A. Ghosh, K. Dey, S. Sabyasachi, A. Karmakar, S. Majumdar, and S. Giri, Appl. Phys. Lett. **103**, 052412 (2013).

[34] R. Prakash, R. J. Choudhary, L. S. Sharath Chandra, N. Lakshmi, and D. M. Phase, J. Phys.: Condensed Matter **19**, 486212 (2007).

[35] R. Master, R. J. Choudhary, and D. M. Phase, J. Appl. Phys. **108**, 103909 (2010).

[36] K. Matsuzaki, V. K. Lazarov, L. Lari, H. Hosono, and T. Susaki, J. Phys. D: Appl. Phys. **46**, 022001 (2013).

[37] T. Tsuchiya, K. Terabe, M. Ochi, T. Higuchi, M. Osada, Y. Yamashita, S. Ueda, and M. Aono, ACS Nano **10**, 1655 (2016).

[38] H.C. Wu, R. Ramos, R. G. S. Sofin, Z.M. Liao, M. Abid, and I. V. Shvets, Appl. Phys. Lett. **101**, 052402 (2012).

[39] J. J. Krebs, D. M. Lind, E. Lochner, K. A. Shaw, W. Portwine, and S. D. Berry, J. Appl. Phys. **75**, 6688 (1994).

[40] H. C. Wu, M. Abid, B. S. Chun, R. Ramos, O. N. Mryasov, and I. V. Shvets, Nano Lett **10**, 1132 (2010).

[41] S. K. Arora, H.C. Wu, R. J. Choudhary, I. V. Shvets, O. N. Mryasov, H. Yao, and W. Y. Ching, Phys Rev B **77,** 134443 (2008).

[42] P. K. J. Wong, W. Zhang, X. G. Cui, Y. B. Xu, J. Wu, Z. K. Tao, X. Li, Z. L. Xie, R. Zhang, and G. van der Laan, Phys. Rev. B **81,** 035419 (2010).

## Figure caption

**Fig. 1.** (a) RHEED pattern of MgO (100) substrate with quasi-2D surface structure. (b) RHEED pattern of $Fe_3O_4$/MgO grown at high vacuum ($\sim 1 \times 10^{-8}$ mbar) with quasi-2D surface structure. The new pattern of line 2 and 4 representing the growth of $Fe_3O_4$. (c) The distance ratio between line 2 and 3 from (b) and the line width of line 2 depending on different oxygen pressure.

**Fig. 2.** (a) XPS and (b) Raman spectra of $Fe_3O_4$ films grown under different oxygen pressures. Inset of (a) is the enlarged view of dotted box.

**Fig. 3.** (a) The schematic structure for magnetotransport measurements in $Fe_3O_4$ films. (b) Resistance versus temperature of $Fe_3O_4$ films grown at pure vacuum and oxygen pressure of $1 \times 10^{-5}$ mbar. Inset is the log resistance versus inverse of temperature $Fe_3O_4$ films grown at pure vacuum. (c) Magnetoresistance versus magnetic field of $Fe_3O_4$ film grown at pure vacuum. (d) Magnetoresistance versus magnetic field of $Fe_3O_4$ film grown at oxygen pressure of $1 \times 10^{-5}$ mbar.

**Fig. 4.** In plane (a) and out plane (b) magnetic hysteresis loops of $Fe_3O_4$ films grown at different oxygen pressures measured at room temperature. (c) In plane and out plane loops of $Fe_3O_4$ films grown at pure vacuum. (d) Saturated magnetic moment and coercivity extract from (a) and (b).
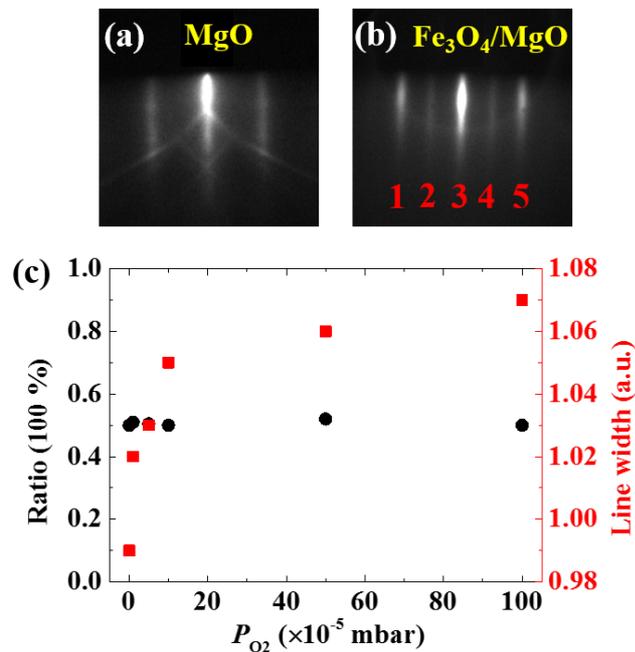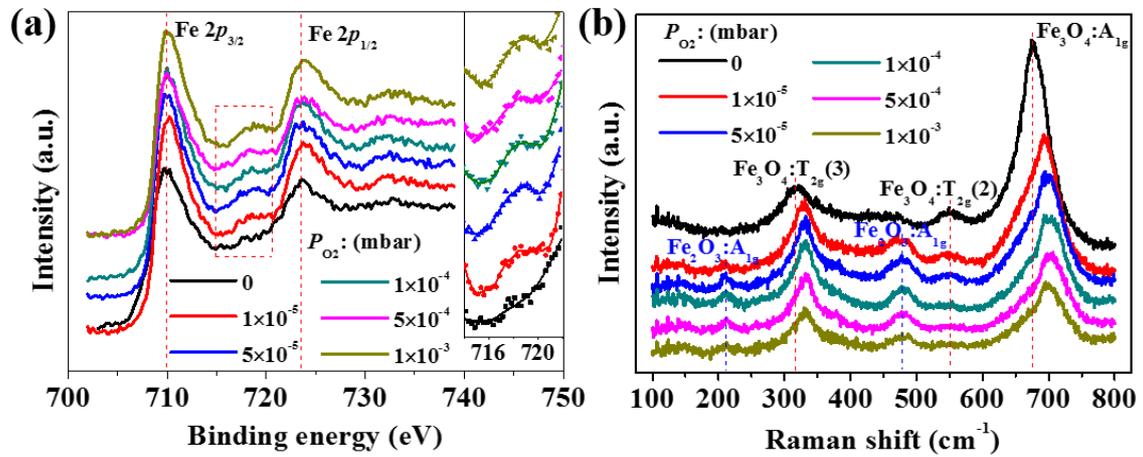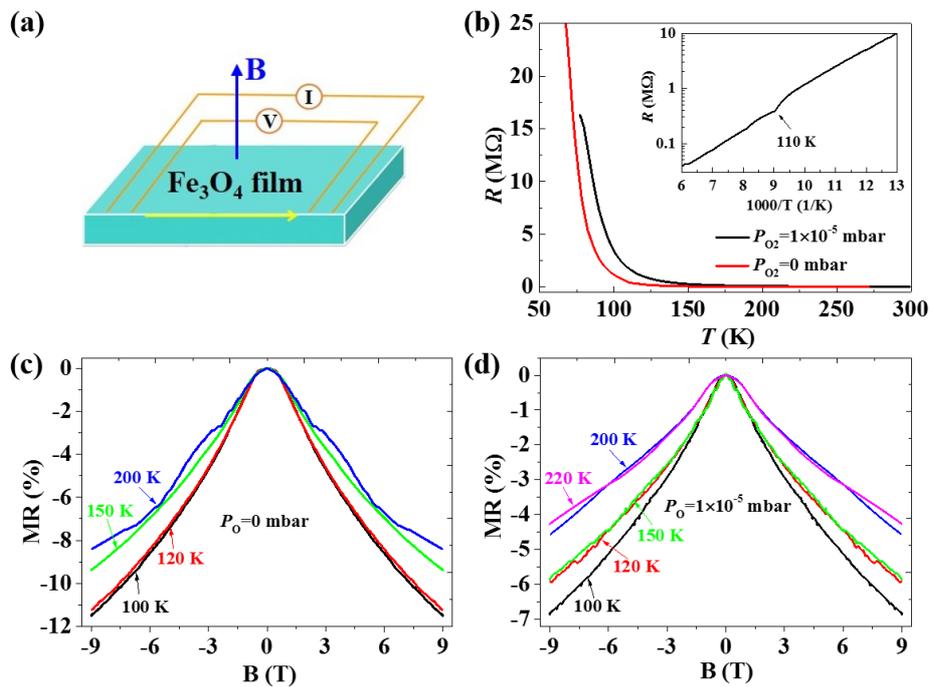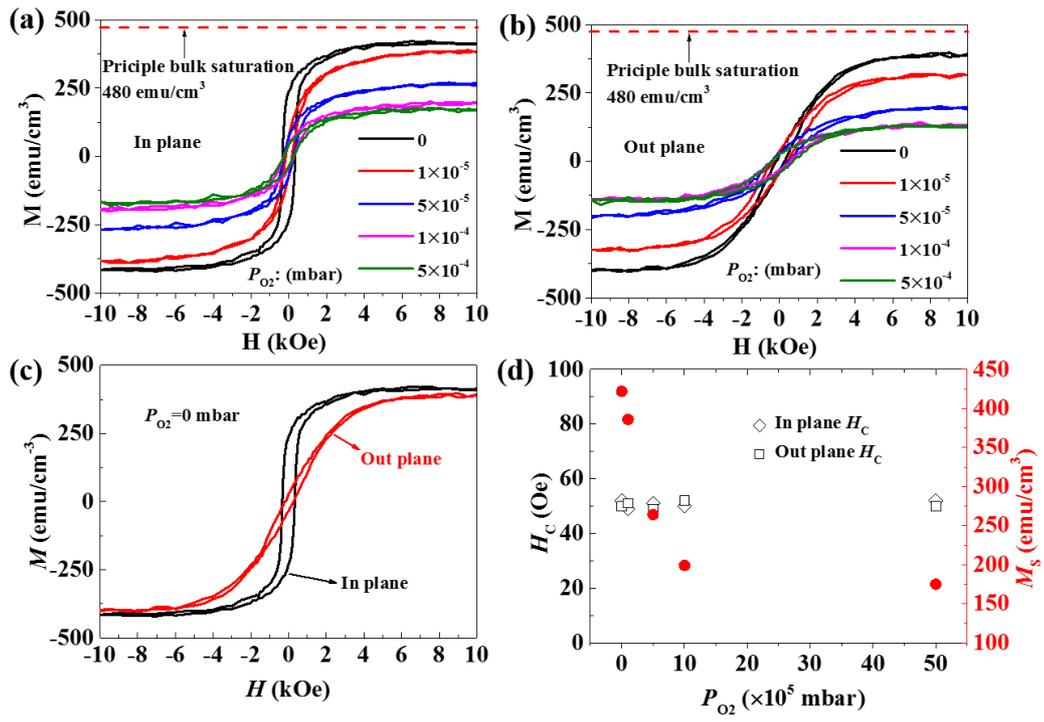


**Fig. 1.**

**Fig. 2.**



**Fig. 3.**

**Fig. 4.**